ACS APPLIED MATERIALS & INTERFACES

Research Article

www.acsami.org

Hierarchical ZnO–Ag–C Composite Porous Microspheres with Superior Electrochemical Properties as Anode Materials for Lithium Ion Batteries

Qingshui Xie, Yating Ma, Deqian Zeng, Xiaoqiang Zhang, Laisen Wang, Guanghui Yue, and Dong-Liang Peng*

Fujian Key Laboratory of Advanced Materials, Collaborative Innovation Center of Chemistry for Energy Materials, Department of Materials Science and Engineering, College of Materials, Xiamen University, Xiamen 361005, China

ABSTRACT: Hierarchical ZnO–Ag–C composite porous microspheres are successfully synthesized by calcination of the preproduced zinc–silver citrate porous microspheres in argon. The carbon derives from the in situ carbonization of carboxylic acid groups in zinc–silver citrate during annealing treatment. The average particle size of ZnO–Ag–C composite porous microspheres is approximate 1.5 μm. When adopted as the electrode materials in lithium ion batteries, the obtained composite porous microspheres display high specific capacity, excellent cyclability, and good rate capability. A discharge capacity as high as 729 mA h g^{-1} can be retained after 200 cycles at 100 mA g^{-1}. The excellent electrochemical properties of ZnO–Ag–C are ascribed to its unique hierarchical porous configuration as well as the modification of silver and carbon.

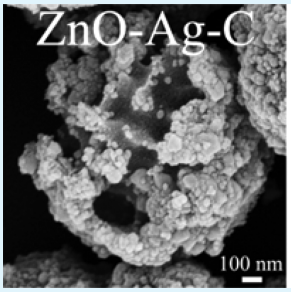

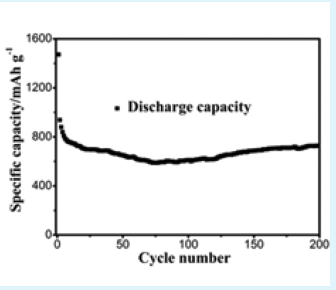

KEYWORDS: *zinc oxide, silver, carbon, hierarchical porous microspheres, lithium ion batteries*

INTRODUCTION

In recent years, rechargeable lithium ion batteries have received more and more attention for use as the predominant power sources for personal electronic devices such as mobile phones, laptop computers, cameras, and so on in view of their special merits of high energy and power density, no memory effect, long cycle time, as well as environment benignity.[1−6] The conventional carbonaceous anodes deliver a low theoretical capacity of 372 mA h g^{-1} which cannot meet the increasingly high energy requirements in electric vehicles or hybrid electric vehicles in future. Moreover, the very low operating potential after Li complete intercalation would give rise to the formation of the dendritic lithium on the surface of carbonaceous electrodes during subsequent deintercalation process, which is an unavoidable safety problem.[7,8] Over the past decade, transition metal oxides have been widely investigated as the alternative anode materials in lithium ion batteries because of their higher theoretical capacity and safety in comparison with traditional carbon materials.[9−14] Among them, ZnO holds bright prospects as the advanced electrode materials since it can react with Li both through the conversion reaction and alloying reaction to contribute to a large theoretical capacity of 978 mA h g^{-1}, besides the advantages of rich resource, friendliness to environment, easy fabrication, and nontoxic.[15] However, ZnO electrodes always suffer the severe capacity fading and bad cycling stability which originated from the huge volume variation during Li insertion/extraction process and the intrinsic poor electronic conductivity. These fatal shortcomings would greatly hamper its potential applications in lithium ion batteries. So, it is of great significance to improve the specific capacity and cyclability of ZnO anodes.

Previous studies have demonstrated that the specific capacity and cycling stability of transition metal oxide anodes can be effectively strengthened through appropriate morphological construction and metal and/or carbon modification.[16−21] Also, considerable attention has been paid to enhance the electrochemical properties of ZnO electrodes.[11,22−26] For example, Shen et al. successfully synthesized ZnO–C powders by a facile solvothermal route, which showed a high reversible capacity of 654 mA h g^{-1} after 100 cycles at 100 mA g^{-1}.[22] Zhu's group reported that the hierarchical flower-like Au–ZnO hybrid nanoparticles possessed better electrochemical performance than single ZnO powders.[26] In our previous work, ZnO–C yolk–shell microspheres delivered the highest discharge capacity as compared to hollow and solid counterparts after 150 cycles.[11] Although some progress has been made, there is still a great deal of space to further improve the electrochemical properties of ZnO electrodes in specific capacity and cyclability.

In this work, hierarchical zinc–silver citrate porous microsphere precursors were synthesized through a facile aging process of the preproduced zinc citrate solid microspheres in silver nitrate solution at room temperature. Afterward, the

Received: August 9, 2014
Accepted: October 28, 2014
Published: October 28, 2014

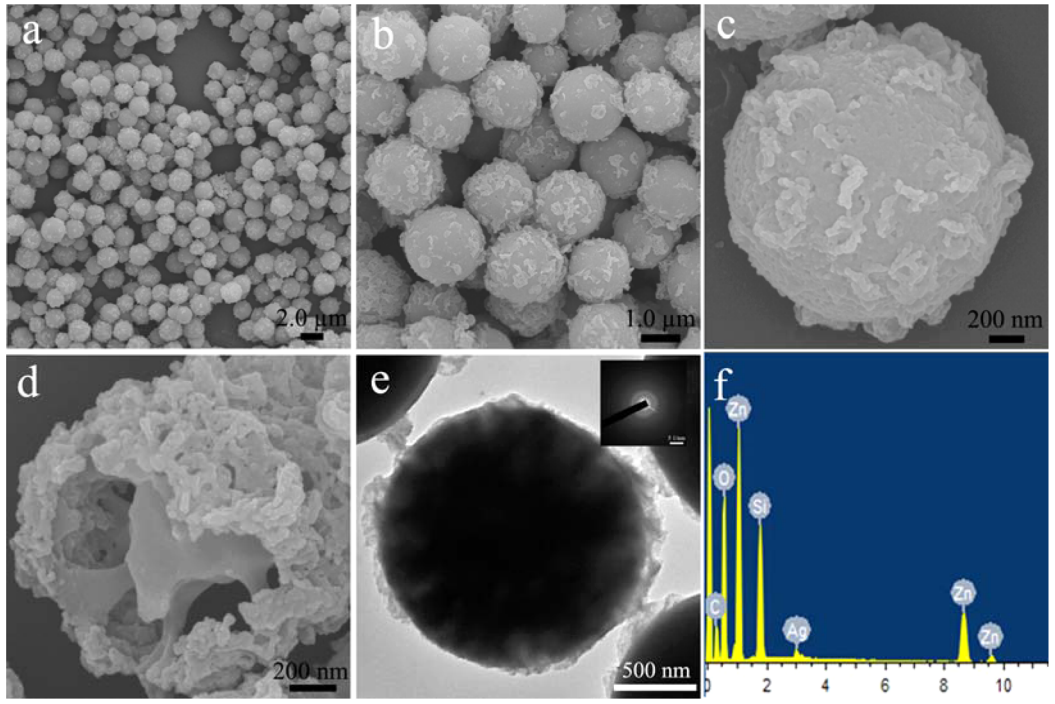

Figure 1. SEM (a–d), TEM (e), and EDS (f) images of hierarchical zinc–silver citrate porous microspheres. The inset in part e is the SAED pattern of an individual microsphere.

acquired precursor was annealed at 500 °C in argon to generate hierarchical ZnO–Ag–C porous microspheres with good morphological inheritance. The carbon derives from the in situ carboxylic acid groups in zinc–silver citrate during carbonization treatment. When employed as the anode materials for lithium ion batteries, hierarchical ZnO–Ag–C porous microspheres reveal exceptional electrochemical performance which is attributed to their hierarchical porous structures and decoration of silver and carbon.

EXPERIMENTAL SECTION

Synthesis. In a typical fabrication process, zinc citrate solid microspheres were first prepared according to our previous report.[27] The presynthesized 0.06 g of zinc citrate solid microspheres was added to 30 mL of silver nitrate (0.003 mol) solution under ultrasonication and then aged at room temperature for 1 h. Thereafter, hierarchical zinc–silver citrate porous microspheres could be collected by centrifugation and rinsed thoroughly with deionized water along with subsequent drying treatment at 60 °C overnight under vacuum condition. The collected zinc–silver citrate porous microspheres were heated at 500 °C for 2 h in argon to synthesize the hierarchical ZnO–Ag–C composite porous microspheres.

Characterizations. X-ray diffraction was collected on a PANalytical X′ pert PRO X-ray diffractometer (Cu Kα radiation 40 kV, 30 mA). The SEM and TEM images of the acquired products were gained from scanning electron microscopy (Hitachi SU-70) and transmission electron microscopy (JEM-2100, 200 kV). Fourier-transform infrared (FTIR) spectrum of zinc–silver citrate was collected from a Nicolet Nexus-670 FT-IR spectrometer. N_2 adsorption–desorption measurement was carried out on a TriStar 3020 system. The carbon content of ZnO–Ag–C composite microspheres was determined by the thermogravimetric (TG) characterization implemented on a SDT-Q600 thermal analyzer. PHI QUANTUM 2000 was employed for XPS tests.

Electrochemical Measurements. The active materials (the produced hierarchical ZnO–Ag–C composite porous microsperes, 70 wt %), acetylene black (20 wt %) and poly(vinyl difluoride) (PVDF, 10 wt %) were dispersed in 1-methyl-2-pyrrolidinone (NMP) to form a homogeneous slurry which was subsequently coated on a copper foil (d = 16 mm) to prepare the working electrode. The loading density of active materials on the copper foil is about 1 mg cm^{-2}. Lithium foil was adopted as the counter electrode and reference electrode. The coin cells (2025-type) were manipulated in an argon-filled glovebox using Celgard 2400 and 1 M $LiPF_6$ dissolved in a mixture consisting of ethylene carbonate (EC) and diethyl carbonate (DEC) (1:1, v/v) as the separator and electrolyte, respectively. Cyclic voltammetry evaluations and electrochemical impedance spectroscopy were performed on an Autolab electrochemical workstation (NOVA 1.9). The galvanostatic discharge–charge investigations were conducted on a Neware battery tester.

RESULTS AND DISCUSSION

The SEM and TEM characterizations were carried out to disclose the morphology and structure of the acquired zinc–silver citrate precursor. From the panoramic SEM observation shown in Figure 1a, the zinc–silver citrate precursor has the microspherical morphology with good dispersion. The average diameter of the microspheres is about 1.9 μm. The high-magnified SEM images (Figure 1b,c) indicate the coarse and loose surface of zinc–silver citrate microspheres, differentiating from the initial zinc citrate solid microspheres which have the rather smooth surfaces (shown in our earlier literature[27]). Interestingly, the inner free cavities can be obviously distinguished from a broken microsphere revealed in Figure 1d, suggesting the hierarchical porous configuration of the synthesized zinc–silver citrate microspheres. Energy dispersive spectroscopy (EDS) measurements (Figure 1f) provide evidence for the presence of Zn, Ag, O, and C elements with a Ag/Zn molar ratio of about 0.047, implying the very low content of silver in the hierarchical zinc–silver citrate porous microspheres. Shown in Figure 1e is the TEM image of zinc–silver citrate microspheres. The contrast between the pale and the dark regions within the microsphere further verifies its hierarchical porous structure. The SAED pattern (the inset in

Figure 1e) demonstrates the amorphous characteristic of the hierarchical zinc−silver citrate porous microspheres, agreeing well with the XRD result shown in Figure 2. This phenomenon hints that the initial amorphous nature of zinc citrate solid microspheres does not change after silver decoration.

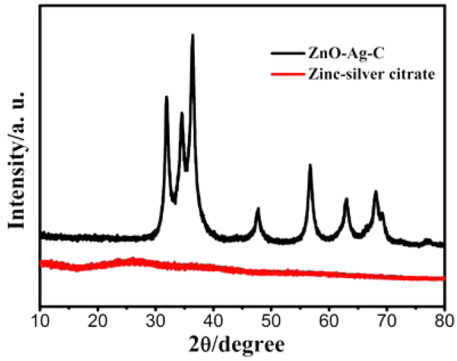

Figure 2. XRD patterns of zinc−silver citrate porous microspheres (a) and ZnO−Ag−C composite porous microspheres (b).

The FT-IR investigation of zinc−silver citrate was performed, and the corresponding result is revealed in Figure 3a. Two intense peaks near 1576.7 and 1398.2 cm^{-1} are associated with the stretching vibrations of carboxylate acid groups ($-COO^-$).[27,28] The broad peak around 3400 cm^{-1} derives from the −OH groups. The presence of Zn, Ag, O, and C elements in zinc−silver citrate is further corroborated from the full XPS spectrum plotted in Figure 3b. Two high-resolution peaks around 1044.6 and 1021.5 eV result from Zn $2p_{1/2}$ and Zn $2p_{3/2}$ of Zn^{2+}, respectively (Figure 3c). Peaks at 367.2 and 373.2 eV in Figure 3d are ascribed to Ag $3d_{5/2}$ and Ag $3d_{3/2}$ of Ag^+, respectively.[29] With all of the above observations and analysis under consideration, it is reasonable to conclude that amorphous hierarchical zinc−silver citrate porous microspheres can be successfully synthesized through a facile aging process of amorphous zinc citrate solid microspheres in silver nitrate solution at room temperature.

After heat treatment of the obtained hierarchical zinc−silver citrate porous microspheres at 500 °C for 2 h in argon, ZnO−Ag−C composite microspheres with good morphological inheritance can be produced for the first time. Figure 2 displays the XRD pattern of the acquired ZnO−Ag−C composites, from which all the diffraction peaks can be assigned to hexagonal ZnO (JCPDS card no. 36-1451). No diffraction peaks originating from Ag and C can be discerned, which may be due to the very low content of Ag (the EDS results shown in Figures 1f and 4j) and the amorphous nature of such derived carbon using carboxylic acid groups as the in situ carbon sources during carbonation process, respectively. The absence of other additional diffraction peaks indicates the good purity of the ZnO−Ag−C composites. The crystallite size of ZnO is about 13.7 nm calculated by the Scherrer equation. The SEM and TEM images of ZnO−Ag−C composites are demonstrated in Figure 4. The sample is dominated by well-dispersed microspheres with particle size on the order of 1.5 μm (Figure 4a). The obtained ZnO−Ag−C composite microspheres have a slight contraction in size compared to hierarchical zinc−silver citrate porous microsphere precursors. A close-up SEM image displayed in Figure 4b implies the rough surfaces of the microspheres which are made up of numerous nanoparticles with size ranging from 5 to 30 nm. Figure 4c exhibits a cracked microsphere, from which the interior void cavities can be visibly distinguished, indicating the good morphological inheritance of the sample after calcination. From the TEM images (Figure 4 d,e), the hierarchical porous

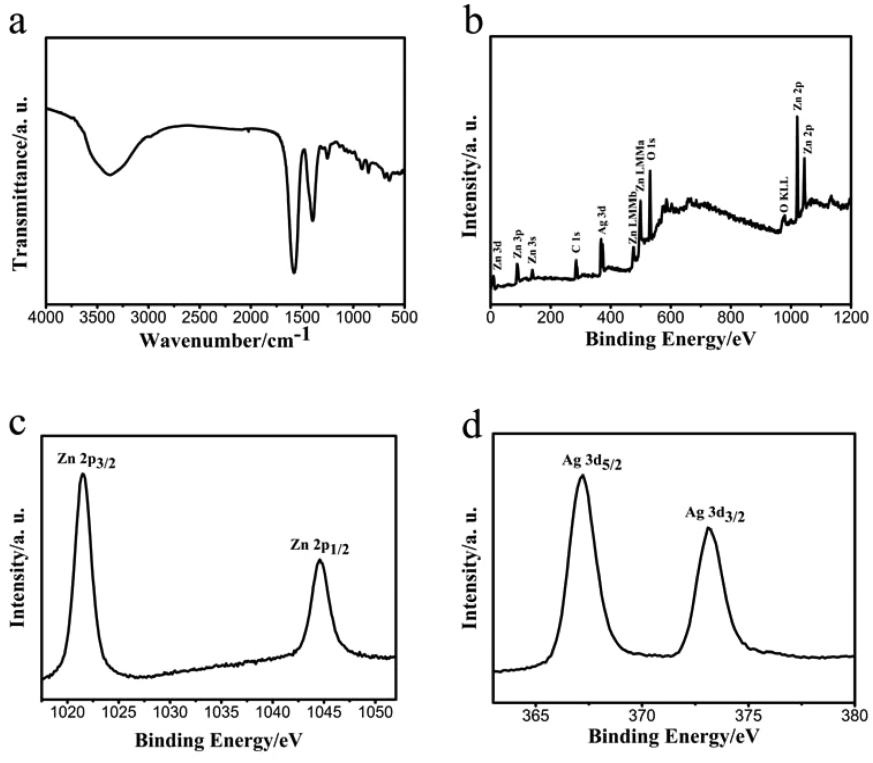

Figure 3. (a) FT-IR spectrum of zinc−silver citrate. The full XPS spectrum (b), high-resolution spectra of Zn (c), and Ag (d) for zinc−silver citrate.

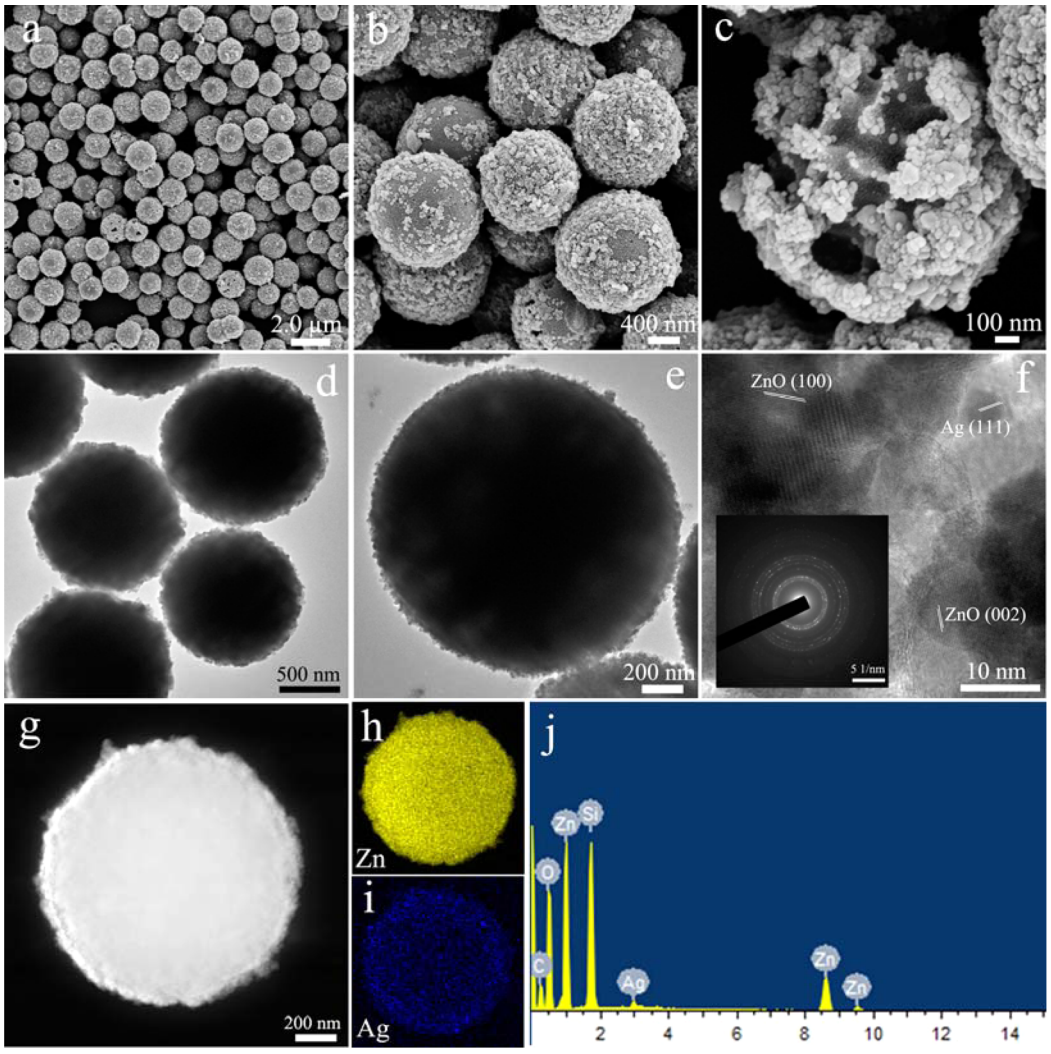

Figure 4. SEM (a–c), TEM (d–e), and HRTEM (f) micrographs of hierarchical ZnO–Ag–C composite porous microspheres. HAADF STEM image (g) and the elemental mappings of Zn (h) and Ag (i) of an individual ZnO–Ag–C porous microsphere. The EDS image (j) of ZnO–Ag–C composite porous microspheres. The inset in part f is the SAED pattern of an individual ZnO–Ag–C composite porous microsphere.

configuration of ZnO–Ag–C composite microspheres can be further carefully visualized by the pale and the dark contrast difference throughout the microspheres, regardless of the big size of the microspheres. The SAED pattern shown in the inset in Figure 4f suggests the polycrystalline characteristic of ZnO–Ag–C composite porous microspheres. HRTEM micrograph in Figure 4f manifests the lattice fringes with the interplanar distances of about 0.281, 0.260, and 0.235 nm which can be assigned to the (100) and (002) planes of ZnO and (111) planes of Ag, respectively. The HRTEM results verify the formation of metallic Ag. The carboxylic acid groups in zinc–silver citrate may convert Ag^+ to metallic Ag due to their reduction ability during the annealing process. The presence of carbon is further corroborated by the TG measurement displayed in Figure 6a which manifests a mass loss of about 11.0% during heating treatment in air. The high-angle annular dark-field (HAADF) scanning TEM (STEM) image (Figure 4g) and the element mappings (Figure 4h,i) reveal the homogeneous distribution of Zn and Ag on the surface of the microsphere. Compared to zinc–silver citrate precursor, the Ag/Zn molar ratio in ZnO–Ag–C composites almost does not change after calcination (Figures 1f and 4j). The accurate contents of ZnO, Ag, and C are 87.62, 1.03, and 11.35 wt %, respectively, measured by the inductively coupled plasma mass spectrometry. According to the above observations and analysis, a schematic formation process of ZnO–Ag–C porous microspheres is illustrated in Figure 5. First, the –OH and $-COO^-$ groups on the surfaces of zinc citrate solid microspheres (FT-IR results in Figure 3a) would adsorb Ag^+ due to the electrostatic interactions during the aging process of zinc citrate solid microspheres in silver nitrate solution. Then, a very thin zinc–silver citrate layer would form at the outermost surface of the microsphere. The smooth surface of microspheres becomes rough and loose at this stage. Further increasing the aging time, the incomplete Ostwald ripening process occurs at a particular region underneath the coarse and loose zinc–silver citrate layer of the solid microspheres, giving rise to the generation of the hierarchical zinc–silver citrate porous microspheres. By calcination of the obtained zinc–silver citrate porous microspheres at 500 °C in argon, hierarchical ZnO–Ag–C composite porous microspheres with good morphological inheritance can be prepared successfully. The carbon derives from the in situ carbonization of carboxylic acid groups in zinc citrate during annealing treatment. The surface of the composite porous microsphere consists of ZnO, Ag, and C nanoparticles, which contact each other tightly. Also, the

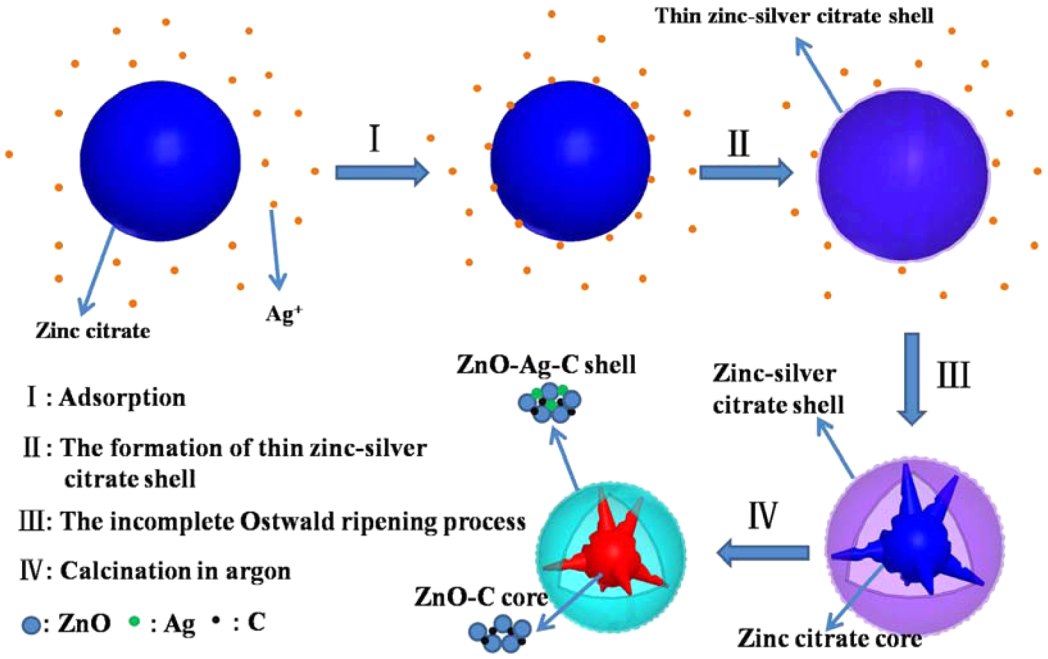

Figure 5. Schematic formation process of ZnO−Ag−C composite porous microspheres.

inner part of the microsphere is made up of ZnO and C nanoparticles, which also contact closely.

N_2 adsorption−desorption investigation at 77 K was performed to elucidate the specific surface area and pore characteristic of the produced hierarchical ZnO−Ag−C porous microspheres. The representative type IV isotherm profile (Figure 6b) suggests the mesoporous structures of ZnO−Ag−C composite microspheres. The specific surface area of the composite microspheres is approximately 103.5 $m^2\ g^{-1}$. The pore size distribution (Figure 6c) calculated by the Barrett−Joyner−Halenda method shows two type pores, including the micropores centered at 1.7 nm and mesopores located at 7.3 nm. These pores may be caused by the release of gas that originated from the decomposition of organic groups (citrate acid groups, $-C_6H_5O7_3^-$) during the carbonation process. It is well-known that the high surface area and porous structures of the active materials can increase the contact area between the electrode and the electrolyte and offer pathways for electrolyte diffusion to the interior surfaces of the active materials, with the consequent benefit of strengthening the electrochemical performance of electrode materials.[4,30−32]

The electrochemical measurements of the hierarchical ZnO−Ag−C composite porous microspheres were implemented. To shed light on the electrode reactions during Li insertion/extraction process, cyclic voltammetry (CV) characterization was carried out at 0.1 mV s^{-1} in 0.01−3 V. As shown in Figure 7a, a large and broad cathodic peak centered at 0.29 V can be seen distinctly in the first lithiation process, arising from the reduction of ZnO to Zn, the alloying reaction between Zn and Li to generate the Zn−Li alloys, and the formation of solid electrolyte interphase (SEI) films.[22,26,33] In the following cycles, this cathodic peak shifts to the higher potential, which may be interpreted by the enhanced kinetics of the electrode reactions after the initial cycle.[33−36] There are three anodic peaks located at 0.30, 0.55, and 0.69 V in the first delithiation process, relating to the multistep dealloying reactions of Zn−Li alloys.[37] The regeneration of ZnO is corroborated by the oxidation peak near 1.34 V in the first anodic sweep.[38] No redox peaks resulting from Ag can be detected because Ag is inactive to Li and only serves as the electronic additive to enhance the electronic conductivity of the electrode materials.[39] After first cycle, the CV profiles have a good superposition in shape, representing that the electrochemical reactions proceed reversibly in the following cycles. On the basis of the above results and analysis, the electrode reactions taken place during the repeated Li uptake/removal process can be concluded as follows:

$$ZnO + 2Li^+ + 2e^- \leftrightarrow Zn + Li_2O \quad (1)$$

$$Zn + xLi^+ + xe^- \leftrightarrow Li_xZn \quad (x \le 1) \quad (2)$$

Figure 7b displays the galvanostatic discharge−charge curves of hierarchical ZnO−Ag−C composite porous microspheres tested at a current density of 100 mA g^{-1} in 0.01−3.0 V. There are two obvious plateau located at 0.7 and 0.5 V in the initial discharge profile. The plateau near 0.7 V corresponds to the SEI formation caused by the decomposition of electrolyte, and the plateau around 0.5 V is associated with the generation of Zn and Li_2O by the reduction of ZnO, which is similar to other ZnO electrodes containing carbon or carbonaceous materials.[25,40,41] The small plateau around 0.2 V may be caused by the alloying reactions of Zn and Li to form Zn−Li alloys.[41,42] In the initial charge curve, two weak plateaus near 0.3 and 0.55 V are related to the dealloying process of Zn−Li alloys, while the weak plateau around 1.3 V corresponds to the reformation of ZnO. These electrochemical phenomena are in accordance with the above CV results (Figure 7a). Hierarchical ZnO−Ag−C composite porous microspheres deliver the first discharge and charge capacities of 1471 and 894 mA h g^{-1}, respectively, producing a Coulombic efficiency of approximate 60.8%. The generation of SEI layers accounts for the irreversible capacity loss during the first cycle, which is the characteristic of most of metal oxide anodes.[43,44] In the subsequent cycles, the similar potential curves concomitant with the increasing Coulombic efficiencies from 91.0% (second cycle), to 93.9% (third cycle), to 98.8% (10th cycle) enlighten us that the electrode reactions take place more reversibly upon cycling. Compared to yolk−

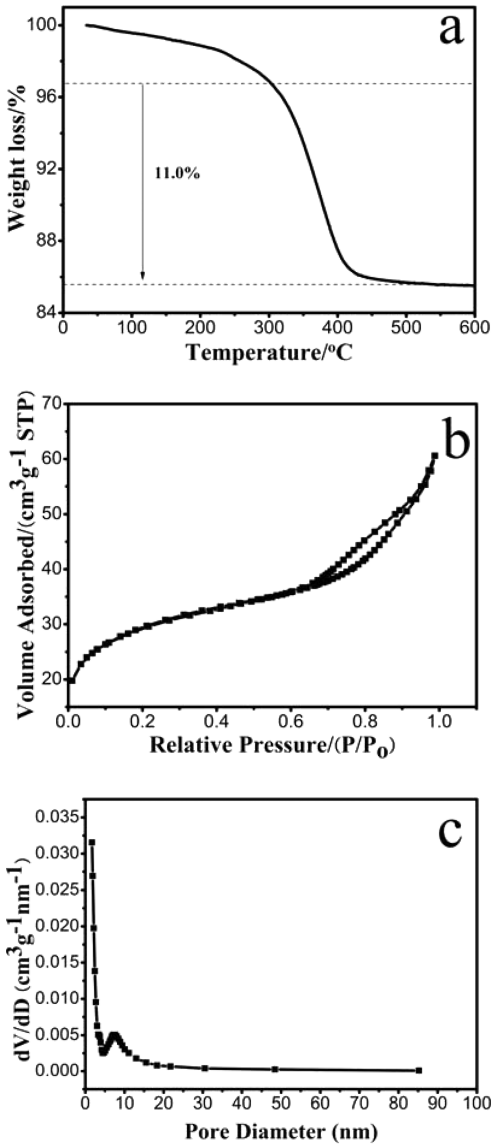

Figure 6. TGA curve (a), N_2 adsorption−desorption isotherms (b), and the pore size distribution (c) of ZnO−Ag−C composite porous microspheres.

shell ZnO−C microspheres reported in our earlier literature, the as-produced ZnO−Ag−C porous microspheres revealed the higher Coulombic efficiency and smaller irreversible capacity lost during the first cycle.[11] The modification of Ag is capable of suppressing the degradation of solvent on the surface of the anode, which is responsible for the increased Coulombic efficiency of ZnO−Ag−C porous microspheres during the first cycle.[45,46]

The cycling performance of the hierarchical ZnO−Ag−C porous microspheres was investigated at 100 mA g^{-1} in 0.01−3.0 V. Apparently, there is a large capacity fading in the first 10 cycles. However, in the subsequent cycles, the specific capacity decreases slowly (Figure 7c). Interestingly, the specific capacity of ZnO−Ag−C porous microspheres slightly increases from 75 cycles until 200 cycles. This phenomenon may be ascribed to the reversible generation and dissolution of polymeric gel-like film caused by kinetically activated electrolyte decomposition during cycling, which contributes to extra specific capacity.[47−49] A high reversible capacity of 729 mA h g^{-1} can be retained for hierarchical ZnO−Ag−C porous microspheres after 200 cycles, which are superior to most of the reported ZnO or ZnO-based anodes summarized in Table 1. For example, flower-like Au−ZnO powders prepared by Zhu's group delivered a specific capacity of 392 mA h g^{-1} after 50 cycles at 120 mA g^{-1}.[26] In our previous work, ZnO−C yolk−shell, hollow and solid composite microspheres were synthesized by a facile strategy, which revealed the discharge capacities of 520, 427, and 341 mA h g^{-1}, respectively, after 150 cycles at a current density of 100 mA g^{-1}.[11] Recently, Shen et al. reported that a high specific capacity of 654 mA h g^{-1} can be achieved for ZnO-loaded/porous carbon composites after 100 cycles at 100 mA g^{-1}.[22] In addition, the cycling performance of the hierarchical ZnO−Ag−C porous microspheres at a high current rate of 500 mA g^{-1} in 0.01−3.0 V is also investigated. From Figure 8, one can clearly observe that the specific capacity decreases quickly in the first 12 cycles and then changes slightly in the following cycles, indicating the good cycling stability of ZnO−Ag−C porous microspheres even at high current rate. After 50 cycles, a specific capacity of about 443 mA h g^{-1} can be retained, which is still higher than the theoretical capacity value (372 mA h g^{-1}) of the conventional carbonaceous anodes.

The outstanding rate capability of the hierarchical ZnO−Ag−C composite porous microspheres can be found from Figure 7d, wherein the reversible capacity gradually decreases as increasing the current rate. Hierarchical ZnO−Ag−C composite porous microspheres deliver the average discharge capacities ranging from 806, 627, 556, 484, 432, to 306 mA h g^{-1} as the current densities increasing from 100, 200, 300, 400, 500 to 1000 mA g^{-1}. A discharge capacity as high as 626 mA h g^{-1} can be still retained with the current density returning to 100 mA g^{-1}. Compared to yolk−shell ZnO−C composite microspheres prepared in our early work, hierarchical ZnO−Ag−C composite porous microspheres exhibit significantly enhanced rate capability, especially in high current rate.[11] In order to show the merits of the modification of Ag, the electrochemical impedance spectra (EIS) of ZnO−Ag−C porous microspheres and yolk−shell ZnO−C microspheres before cycling are tested, and the results are displayed in Figure 9a. A depressed semicircle in the high-to-medium frequency and a slope in the low frequency region can be seen visibly. The diameter of the semicircle represents the charge transfer resistance (R_{ct}). Distinctly, after decoration of metal Ag, the charge transfer resistance of the active materials is reduced greatly, implying the improvement of electronic conductivity of ZnO−Ag−C porous microspheres. The enhanced electronic conductivity is conducive to the fast transport of electron in the microspheres and ensures better electrical contact of active materials with the current collector, which leads to the good lithium storage properties of ZnO−Ag−C porous microspheres at high current rate. Furthermore, the electrochemical impedance spectra (EIS) of ZnO−Ag−C electrodes after different cycles are tested and demonstrated in Figure 9b, wherein all the Nyquist plots have similar shape. Apparently, the R_{ct} value of electrodes increases obviously with the cycle number increasing from 5 to 40 cycles. However, there is only a slight increase in R_{ct} value when the cycle number further increases from 40 to 80 cycles. The increased charge transfer resistance over cycling may originate from the dissolution of the organic polymeric constituents in the initially formed SEI layers into the electrolyte, resultantly decreasing the conductivity of the electrolyte.[52] The structural stability of the electrode materials after cycling was evaluated by SEM. As manifested in

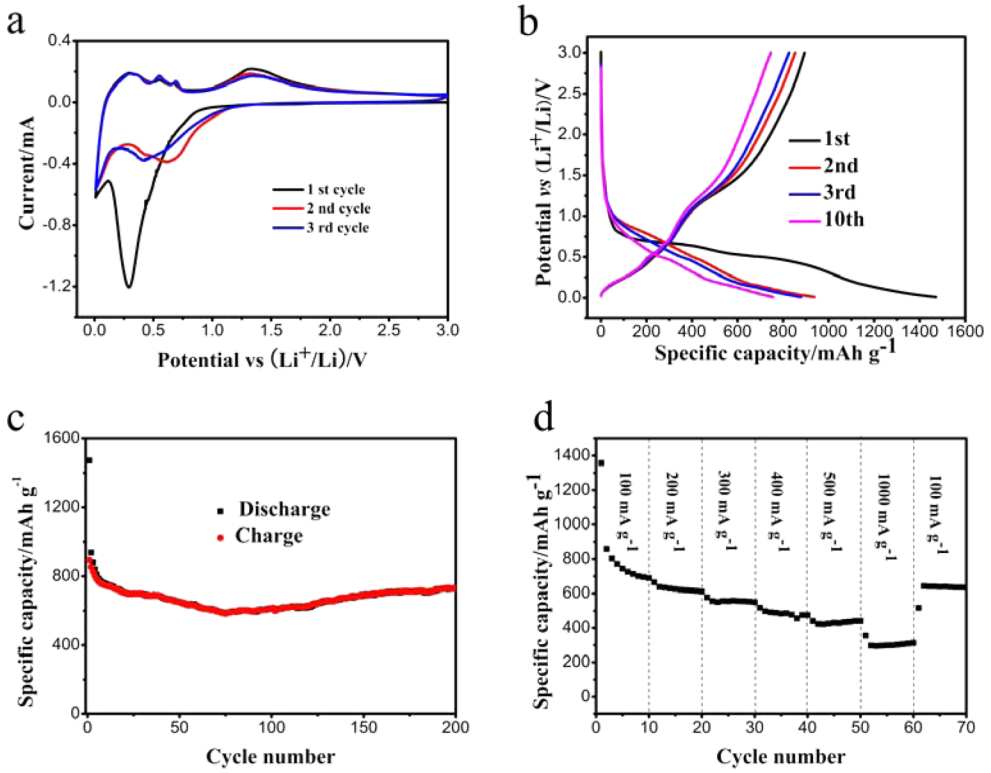

Figure 7. (a) First three cyclic voltammogram curves of ZnO−Ag−C composite porous microspheres measured at 0.1 mV s^{-1} in the potential window 0.01−3 V. (b) The galvanostatic discharge−charge profiles of ZnO−Ag−C porous microspheres at 100 mA g^{-1}. The cycling properties (c) and rate capabilities (d) of ZnO−Ag−C composite porous microspheres.

Table 1. Electrochemical Performances of Various ZnO or ZnO-Based Anode Materials

materials	morphology	reversible capacity/mA h g^{-1}	cycles	ref
ZnO	ultrathin nanotubes	386	50	25
ZnO	dandelion-like nanorod arrays	310	40	33
ZnO	flower-like nanospheres	381	30	43
ZnO	porous nanosheets	400	100	24
ZnO−C	nanorod arrays	330	50	23
ZnO−C	yolk−shell/hollow/solid microspheres	520/427/341	150	11
ZnO−C	particles	654	100	22
ZnO−graphene	nanodisc−nanosheet composites	460	100	50
ZnO−Se	nanocomposites	<400	100	51
ZnO−Au	flower-like nanostructures	392	50	26
ZnO−Ag−C	hierarchical porous microspheres	729	200	this work

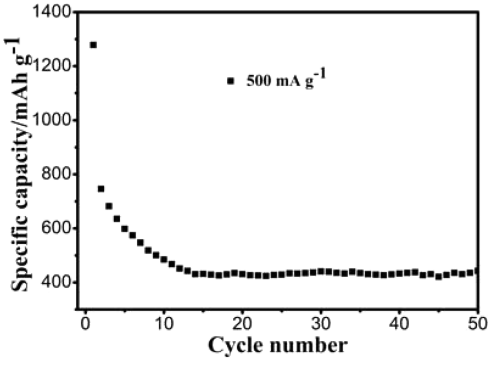

Figure 8. Cycling properties of ZnO−Ag−C composite porous microspheres at a high current rate of 500 mA g^{-1} in 0.01−3 V.

Figure 10, the original microspherical morphology of ZnO−Ag−C composites was basically maintained after 50 cycles at 100 mA g^{-1}. Meanwhile, no obvious agglomeration and pulverization of the active materials can be observed. These behaviors suggest the good structural stability of the hierarchical ZnO−Ag−C composite porous microspheres during the repeated lithium insertion/extraction process.

The exceptional electrochemical properties of ZnO−Ag−C composites can be rationally interpreted by its unique hierarchical porous construction and the incorporation of silver and carbon. First, as we all know, ZnO anode reveals a large volume change (about 228%) during the repeated lithium intercalation/deintercalation process. The mechanical stress resulted from the huge volume variation would lead to the shedding of active materials from the current collector and the pulverization of electrodes, which is fatal for specific capacity and cycling stability of electrodes.[32] The porous structures of the as-obtained ZnO−Ag−C composite microspheres can effectively accommodate the volume change by providing

dx.doi.org/10.1021/am505352p | ACS Appl. Mater. Interfaces 2014, 6, 19895−19904

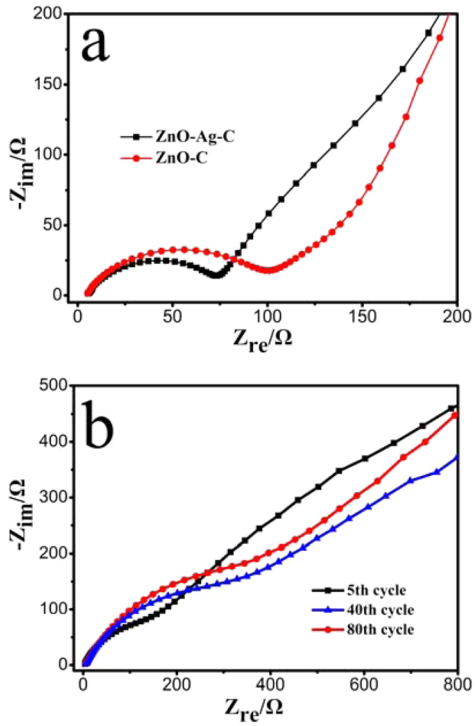

Figure 9. Electrochemical impedance spectra of (a) ZnO–Ag–C composite porous microspheres and yolk–shell ZnO–C microspheres before cycling and (b) ZnO–Ag–C composite porous microspheres after different cycles under a frequency range from 0.1 Hz to 100 kHz.

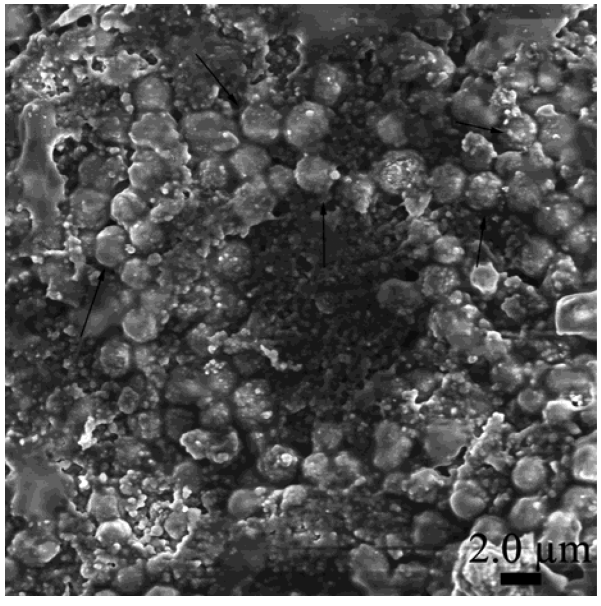

Figure 10. SEM image of ZnO–Ag–C composite porous microspheres after 50 cycles. The black arrows show some of the intact ZnO–Ag–C composite porous microspheres.

some space for expansion during cycling, consequently benefiting the improvement of lithium storage properties. In addition, the micropores and mesopores in the microspheres can facilitate the diffusion of electrolyte into the inner area of the active materials and provide a short Li^+ diffusion pathway, giving rise to the enhanced cyclability.[4,32] Second, the high specific surface area of the hierarchical ZnO–Ag–C composite porous microspheres can offer a large contact area between the electrode materials and the electrolyte and enhance the charge-transfer rate, consequently favoring increase of the specific capacity and rate performance.[19,53] Third, it is well-established that the decoration of silver and carbon is propitious to strengthen the electronic conductivity of active materials, benefiting an improvement of the kinetics of electrochemical reactions.[21−23,39] In addition, the carbon can also increase the structural tolerance of electrode materials during Li intercalation/deintercalation process, which is good for the cycling stability.[54,55] Finally, ZnO–Ag–C composite porous microspheres are made up of numerous nanoparticles. Such hierarchical secondary construction is favorable to reduce the side reactions in the electrodes and ensure good electrical properties.[52] Combining all of the above advantages, the hierarchical ZnO–Ag–C composite porous microspheres show high specific capacity, excellent cycling stability, and good rate capability when used as the anode materials for lithium ion batteries.

CONCLUSIONS

In conclusion, hierarchical ZnO–Ag–C composite porous microspheres were successfully prepared by a facile aging process of zinc citrate solid microspheres in silver nitrate solution with subsequent annealing treatment at 500 °C for 2 h in argon. The carbon derives from the in situ carboxylic acid groups in zinc–silver citrate during the carbonization treatment. The obtained hierarchical ZnO–Ag–C composite porous microspheres possess a large surface area of 103.5 m^2 g^{-1} and numerous nanopores. When applied as the anode materials for lithium ion batteries, ZnO–Ag–C composite porous microspheres deliver a reversible capacity as high as 729 mA h g^{-1} after 200 cycles. The hierarchical porous structures and the modification of silver and carbon are responsible for the excellent electrochemical properties. This facile synthesis strategy can be employed for the fabrication of other ZnO-based porous micro/nanostructures which may hold great promise for advanced anode materials in next-generation lithium ion batteries.

AUTHOR INFORMATION

Corresponding Author

*E-mail: dlpeng@xmu.edu.cn.

Notes

The authors declare no competing financial interest.

ACKNOWLEDGMENTS

The authors gratefully acknowledge financial support from the National Basic Research Program of China (No. 2012CB933103), the National Outstanding Youth Science Foundation of China (Grant No. 50825101), the National Natural Science Foundation of China (Grant Nos. 51171158 and 51371154), and the Fundamental Research Funds for the Central Universities of China (Grant No. 201312G003).

REFERENCES

(1) Armand, M.; Tarascon, J. M. Building Better Batteries. *Nature* **2008**, *451*, 652–657.

(2) Cheng, F.; Tao, Z.; Liang, J.; Chen, J. Template-Directed Materials for Rechargeable Lithium-Ion Batteries. *Chem. Mater.* **2008**, *20*, 667–681.

(3) Chen, J. S.; Archer, L. A.; Lou, X. W. SnO_2 Hollow Structures and TiO_2 Nanosheets for Lithium-Ion Batteries. *J. Mater. Chem.* **2011**, *21*, 9912–9924.

(4) Wang, Z.; Zhou, L.; Lou, X. W. Metal Oxide Hollow Nanostructures for Lithium-Ion Batteries. *Adv. Mater.* **2012**, *24*, 1903−1911.
(5) Tarascon, J. M.; Armand, M. Issues and Challenges Facing Rechargeable Lithium Batteries. *Nature* **2001**, *414*, 359−367.
(6) Bruce, P. G.; Scrosati, B.; Tarascon, J. M. Nanomaterials for Rechargeable Lithium Batteries. *Angew. Chem., Int. Ed.* **2008**, *47*, 2930−2946.
(7) Cai, R.; Yu, X.; Liu, X.; Shao, Z. $Li_4Ti_5O_{12}$/Sn Composite Anodes for Lithium-Ion Batteries: Synthesis and Electrochemical Performance. *J. Power Sources* **2010**, *19*, 8244−8250.
(8) Tang, H.; Tang, Z.; Du, C.; Qie, F.; Zhu, J. Ag-Doped $Li_2ZnTi_3O_8$ as a High Rate Anode Material for Rechargeable Lithium-Ion Batteries. *Electrochim. Acta* **2014**, *120*, 187−192.
(9) Pan, A. Q.; Wu, H. B.; Zhang, L.; Lou, X. W. Uniform V_2O_5 Nanosheet-Assembled Hollow Microflowers with Excellent Lithium Storage Properties. *Energy Environ. Sci.* **2013**, *6*, 1476−1479.
(10) Deng, J.; Yan, C.; Yang, L.; Baunack, S.; Oswald, S.; Wendrock, H.; Mei, Y.; Schmidt, O. G. Sandwich-Stacked SnO_2/Cu Hybrid Nanosheets as Multichannel Anodes for Lithium Ion Batteries. *ACS Nano* **2013**, *7*, 6948−6954.
(11) Xie, Q.; Zhang, X.; Wu, X.; Wu, H.; Liu, X.; Yue, G.; Yang, Y.; Peng, D. L. Yolk-Shell ZnO-C Microspheres with Enhanced Electrochemical Performance as Anode Material for Lithium Ion Batteries. *Electrochim. Acta* **2014**, *125*, 659−665.
(12) Sun, Y.; Hu, X.; Luo, W.; Huang, Y. Porous Carbon-Modified MnO Disks Prepared By a Microwave-Polyol Process and Their Superior Lithium-Ion Storage Properties. *J. Mater. Chem.* **2012**, *22*, 19190−19195.
(13) Wang, Z.; Luan, D.; Madhavi, S.; Hu, Y.; Lou, X. W. Assembling Carbon-Coated α-Fe_2O_3 Hollow Nanohorns on the CNT Backbone for Superior Lithium Storage Capability. *Energy Environ. Sci.* **2012**, *5*, 5252−5256.
(14) Zhuo, L.; Wu, Y.; Ming, J.; Wang, L.; Yu, Y.; Zhang, X.; Zhao, F. Facile Synthesis of a Co_3O_4-Carbon Nanotube Composite and its Superior Performance as an Anode Material for Li-Ion Batteries. *J. Mater. Chem. A* **2013**, *1*, 1141−1147.
(15) Huang, X. H.; Wu, J. B.; Lin, Y.; Guo, R. Q. ZnO Microrod Arrays Grown on Copper Substrates as Anode Materials for Lithium Ion Batteries. *Int. J. Electrochem. Sci.* **2012**, *7*, 6611−6621.
(16) Pan, A.; Wu, H. B.; Yu, L.; Lou, X. W. Template-Free Synthesis of VO_2 Hollow Microspheres with Various Interiors and Their Conversion into V_2O_5 for Lithium-Ion Batteries. *Angew. Chem.* **2013**, *125*, 2282−2286.
(17) Hong, Y. J.; Son, M. Y.; Kang, Y. C. One-Pot Facile Synthesis of Double-Shelled SnO_2 Yolk-Shell-Structured Powders by Continuous Process as Anode Materials for Li-Ion Batteries. *Adv. Mater.* **2013**, *25*, 2279−2283.
(18) Huang, Y.; Huang, X. L.; Lian, J. S.; Xu, D.; Wang, L. M.; Zhang, X. B. Self-Assembly of Ultrathin Porous NiO Nanosheets/Graphene Hierarchical Structure for High-Capacity and High-Rate Lithium Storage. *J. Mater. Chem.* **2012**, *22*, 2844−2847.
(19) Li, J.; Xiong, S.; Li, X.; Qian, Y. A Facile Route to Synthesize Multiporous $MnCo_2O_4$ and $CoMn_2O_4$ Spinel Quasi-Hollow Spheres with Improved Lithium Storage Properties. *Nanoscale* **2013**, *5*, 2045−2054.
(20) Mai, Y. J.; Xia, X. H.; Chen, R.; Gu, C. D.; Wang, X. L.; Tu, J. P. Self-Supported Nickel-Coated NiO Arrays for Lithium-Ion Batteries with Enhanced Capacity and Rate Capability. *Electrochim. Acta* **2012**, *67*, 73−78.
(21) Nam, S. H.; Shim, H. S.; Kim, Y. S.; Dar, M. A.; Kim, J. G.; Kim, W. B. Ag or Au Nanoparticle-Embedded One-Dimensional Composite TiO_2 Nanofibers Prepared via Electrospinning for Use in Lithium-Ion Batteries. *ACS Appl. Mater. Interfaces* **2010**, *2*, 2046−2052.
(22) Shen, X.; Mu, D.; Chen, S.; Wu, B.; Wu, F. Enhanced Electrochemical Performance of ZnO-Loaded/Porous Carbon Composite as Anode Materials for Lithium Ion Batteries. *ACS Appl. Mater. Interfaces* **2013**, *5*, 3118−3125.
(23) Liu, J.; Li, Y.; Ding, R.; Jiang, J.; Hu, Y.; Ji, X.; Chi, Q.; Zhu, Z.; Huang, X. Carbon/ZnO Nanorod Array Electrode with Significantly Improved Lithium Storage Capability. *J. Phys. Chem. C* **2009**, *113*, 5336−5339.
(24) Huang, X. H.; Xia, X. H.; Yuan, Y. F.; Zhou, F. Porous ZnO Nanosheets Grown on Copper Substrates as Anodes for Lithium Ion Batteries. *Electrochim. Acta* **2011**, *56*, 4960−4965.
(25) Park, K. T.; Xia, F.; Kim, S. W.; Kim, S. B.; Song, T.; Paik, U.; Park, W. I. Facile Synthesis of Ultrathin ZnO Nanotubes with Well-Organized Hexagonal Nanowalls and Sealed Layouts: Applications for Lithium Ion Battery Anodes. *J. Phys. Chem. C* **2013**, *117*, 1037−1043.
(26) Ahmad, M.; Shi, Y.; Nisar, A.; Sun, H.; Shen, W.; Wei, M.; Zhu, J. Synthesis of Hierarchical Flower-Like ZnO Nanostructures and Their Functionalization by Au Nanoparticles for Improved Photocatalytic and High Performance Li-Ion Battery Anodes. *J. Mater. Chem.* **2011**, *21*, 7723−7729.
(27) Xie, Q.; Li, J.; Tian, Q.; Shi, R. Template-Free Synthesis of Zinc Citrate Yolk-Shell Microspheres and Their Transformation to ZnO Yolk-Shell Nanospheres. *J. Mater. Chem.* **2012**, *22*, 13541−13547.
(28) Cho, S.; Jang, J. W.; Jung, A.; Lee, S. H.; Lee, J.; Lee, J. S.; Lee, K. H. Formation of Amorphous Zinc Citrate Spheres and Their Conversion to Crystalline ZnO Nanostructures. *Langmuir* **2011**, *27*, 371−378.
(29) Krishnakumar, B.; Subash, B.; Swaminathan, M. AgBr-ZnO-An Efficient Nano-Photocatalyst for the Mineralization of Acid Black 1 with UV Light. *Sep. Purif. Technol.* **2012**, *85*, 35−44.
(30) Liu, J.; Xue, D. Hollow Nanostructured Anode Materials for Li-Ion Batteries. *Nanoscale Res. Lett.* **2010**, *5*, 1525−1534.
(31) Zhao, Y.; Jiang, L. Hollow Micro/Nanomaterials with Multilevel Interior Structures. *Adv. Mater.* **2009**, *21*, 3621−3638.
(32) Vu, A.; Qian, Y.; Stein, A. Porous Electrode Materials for Lithium-Ion Batteries-How to Prepare Them and What Makes Them Special. *Adv. Energy Mater.* **2012**, *2*, 1056−1085.
(33) Wang, H.; Pan, Q.; Cheng, Y.; Zhao, J.; Yin, G. Evaluation of ZnO Nanorod Arrays with Dandelion-Like Morphology as Negative Electrodes for Lithium-Ion Batteries. *Electrochim. Acta* **2009**, *54*, 2851−2855.
(34) Huang, X. H.; Guo, R. Q.; Wu, J. B.; Zhang, P. Mesoporous ZnO Nanosheets for Lithium Ion Batteries. *Mater. Lett.* **2014**, *122*, 82−85.
(35) Kim, J. H.; Kang, Y. C. Electrochemical Properties of Micron-Sized, Spherical, Meso- and Macro-Porous Co_3O_4 and CoO-Carbon Composite Powders Prepared by a Two-Step Spray Drying Process. *Nanoscale* **2014**, *6*, 4789−4795.
(36) Zhang, P.; Guo, Z. P.; Huang, Y.; Jia, D.; Liu, H. K. Synthesis of Co_3O_4/Carbon Composite Nanowires and Their Electrochemical Properties. *J. Power Sources* **2011**, *196*, 6987−6991.
(37) Wu, M. S.; Chang, H. W. Self-Assembly of NiO-Coated ZnO Nanorod Electrodes with Core-Shell Nanostructures as Anode Materials for Rechargeable Lithium-Ion Batteries. *J. Phys. Chem. C* **2013**, *117*, 2590−2599.
(38) Sharma, Y.; Sharma, N.; Rao, G. V. S.; Chowdari, B. V. R. Nanophase $ZnCo_2O_4$ as a High Performance Anode Material for Li-Ion Batteries. *Adv. Funct. Mater.* **2007**, *17*, 2856−2861.
(39) Yu, Y.; Gu, L.; Zhu, C.; Tsukimoto, S.; Aken, P. A.; Maier, J. Reversible Storage of Lithium in Silver-Coated Three-Dimensional Macroporous Silicon. *Adv. Mater.* **2010**, *22*, 2247−2250.
(40) Yu, M.; Wang, A.; Wang, Y.; Li, C.; Shi, G. An Alumina Stabilized ZnO-Graphene Anode for Lithium Ion Batteries via Atomic Layer Deposition. *Nanoscale* **2014**, *6*, 11419−11424.
(41) Sun, X.; Zhou, C.; Xie, M.; Sun, H.; Hu, T.; Lu, F.; Scott, S. M.; George, S. M.; Lian, J. Synthesis of ZnO Quantum Dot/Grapheme Nanocomposites by Atomic Layer Deposition with High Lithium Storage Capacity. *J. Mater. Chem. A* **2014**, *2*, 7319−7326.
(42) Pan, Q.; Qin, L.; Liu, J.; Wang, H. Flower-Like ZnO-NiO-C Films with High Reversible Capacity and Rate Capability for Lithium-Ion Batteries. *Electrochim. Acta* **2010**, *55*, 5780−5785.
(43) Li, F.; Yang, L.; Xu, G.; Huang, X.; Yang, X.; Wei, X.; Ren, Z.; Shen, G.; Han, G. Hydrothermal Self-Assembly of Hierarchical

Flower-Like ZnO Nanospheres with Nanosheets and Their Application in Li-Ion Batteries. *J. Alloys Compd.* **2013**, *577*, 663−668.
(44) Fu, Z. W.; Huang, F.; Zhang, Y.; Chu, Y.; Qin, Q. Z. The Electrochemical Reaction of Zinc Oxide Thin Films with Lithium. *J. Electrochem. Soc.* **2003**, *150*, A714−A720.
(45) He, B. L.; Dong, B.; Li, H. L. Preparation and Electrochemical Properties of Ag-Modified TiO_2 Nanotube Anode Material for Lithium-Ion Battery. *Electrochem. Commun.* **2007**, *9*, 425−430.
(46) Yan, J.; Song, H.; Yang, S.; Yan, J.; Chen, X. Preparation and Electrochemical Properties of Composites of Carbon Nanotubes Loaded with Ag and TiO_2 Nanoparticle for Use as Anode Material in Lithium-Ion Batteries. *Electrochim. Acta* **2008**, *53*, 6351−6355.
(47) Qiao, L.; Wang, X.; Qiao, L.; Sun, X.; Li, X.; Zheng, Y.; He, D. Single Electrospun Porous NiO-ZnO Hybrid Nanofibers as Anode Materials for Advanced Lithium-Ion Batteries. *Nanoscale* **2013**, *5*, 3037−3042.
(48) Bai, Z.; Ju, Z.; Guo, C.; Qian, Y.; Tang, B.; Xiong, S. Direct Large-Scale Synthesis of 3D Hierarchical Mesoporous NiO Microspheres as High Performance Anode Materials for Lithium Ion Batteries. *Nanoscale* **2014**, *6*, 3268−3273.
(49) Xu, S.; Hessel, C. M.; Ren, H.; Yu, R.; Jin, Q.; Yang, M.; Zhao, H.; Wang, D. a-Fe_2O_3 Multi-Shelled Hollow Microspheres for Lithium Ion Battery Anodes with Superior Capacity and Charge Retention. *Energy Environ. Sci.* **2014**, *7*, 632−637.
(50) Hsieh, C. T.; Lin, C. Y.; Chen, Y. F.; Lin, J. S. Synthesis of ZnO@Graphene Composites as Anode Materials for Lithium Ion Batteries. *Electrochim. Acta* **2013**, *111*, 359−365.
(51) Zhou, Y. N.; Li, W. J.; Fu, Z. W. Electrochemical Reactivity of Nanocomposite ZnO-Se for Lithium-Ion Batteries. *Electrochim. Acta* **2012**, *59*, 435−440.
(52) Hu, L.; Zhong, H.; Zheng, X.; Huang, Y.; Zhang, P.; Chen, Q. $CoMn_2O_4$ Spinel Hierarchical Microspheres Assembled with Porous Nanosheets as Stable Anodes for Lithium-Ion Batteries. *Sci. Rep.* **2012**, *2*, 986−993.
(53) Wang, N.; Ma, X.; Xu, H.; Chen, L.; Yue, J.; Niu, F.; Yang, J.; Qian, Y. Porous $ZnMn_2O_4$ Microspheres as a Promising Anode Material for Advanced Lithium-Ion Batteries. *Nano Energy* **2014**, *6*, 193−199.
(54) Yang, Z.; Du, G.; Meng, Q.; Guo, Z.; Yu, X.; Chen, Z.; Guo, T.; Zeng, R. Synthesis of Uniform TiO_2@Carbon Composite Nanofibers as Anode for Lithium Ion Batteries with Enhanced Electrochemical Performance. *J. Mater. Chem.* **2012**, *22*, 5848−5854.
(55) Chen, J. S.; Liu, H.; Qiao, S. Z.; Lou, X. W. Carbon-Supported Ultra-Thin Anatase TiO_2 Nanosheets for Fast Reversible Lithium Storage. *J. Mater. Chem.* **2011**, *21*, 5687−5692.